

Combined neutron and synchrotron studies of magnetic films

SUNIL K SINHA^{1,2}, S ROY¹, M R FITZSIMMONS², S PARK², M DORN¹,
O PETRACIC^{1,3}, I V ROSHCHIN¹, ZHI-PAN LI¹, X BATLLE^{3,4},
R MORALES^{1,5}, A MISRA², X ZHANG², K CHESNEL⁶, J B KORTRIGHT⁶ and
IVAN K SCHULLER¹

¹Department of Physics, University of California at San Diego, La Jolla, CA 92093, USA

²Los Alamos National Laboratory, Los Alamos, NM 87545, USA

³Angewandte Physik, Universität Duisburg-Essen, 47048 Duisburg, Germany

⁴Departament de Física Fonamental, Universitat de Barcelona, 08028 Barcelona,
Catalonia, Spain

⁵Departamento de Física, Universidad de Oviedo, c/Calvo Sotol s/n, Oviedo 33007, Spain

⁶Lawrence Berkeley National Laboratory, Berkeley, CA 94720, USA

E-mail: ssinha@physics.ucsd.edu

Abstract. We discuss specular reflectivity and off-specular scattering of neutrons and X-rays from magnetic films. Both these techniques are capable of providing information about the morphology of the chemical and magnetic roughness and the magnetic domain structure. The use of neutrons with polarization analysis enables the spatial distribution of different vector components of the magnetization to be determined, and the use of resonant magnetic X-ray scattering enables magnetization in a compound system to be determined element-selectively. Thus both these methods provide powerful and complementary new probes for studying magnetism at the nanoscopic level in a variety of systems such as those exhibiting exchange bias, giant magnetoresistance, spin injection, etc. We shall illustrate with an example of both techniques applied to an exchange bias system consisting of a single crystal of antiferromagnetic FeF₂ capped with a ferromagnetic Co film, and discuss what has been learned about how exchange bias works in such a system.

Keywords. Neutron reflectometry; X-ray reflectometry; magnetic films.

PACS Nos 61.12.H; 61.10.K; 75.70.K

1. Introduction

The use of magnetic films in the magnetic recording industry has attracted a lot of interest in the basic physics of magnetic nanostructures. Thus, the discovery of the phenomenon of giant magnetoresistance has led to the introduction of magnetic spin valve devices which are incorporated in almost all magnetic read heads on computer disk drives today. These consist of a pair of ferromagnetic layers coupled antiferromagnetically through an interspersed non-ferromagnetic metallic

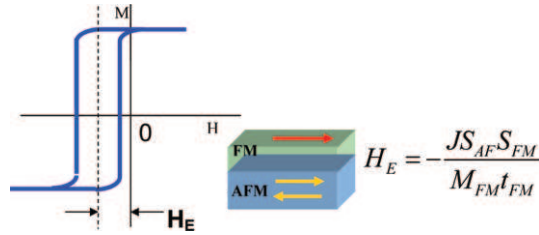


Figure 1. Schematic of conventional picture of exchange bias effect. The shift of the hysteresis loop of the FM is calculated assuming a ferromagnetic coupling of the last ‘uncompensated’ layer of spins of the AF to the adjacent layer of FM spins across the interface assuming a smooth interface.

layer. The reference ferromagnetic layer is pinned while the other layer can change its magnetization direction in response to the magnetic field of the stored bit it is sensing. Since the resistance of such a magnetic sandwich is significantly lower if the two ferromagnetic films are parallel than if they are antiparallel, this leads to a change in resistivity across the read head. This then translates into voltage changes in response to the magnetically stored information. The direction of the reference ferromagnetic layer is pinned via the phenomenon of ‘exchange bias’. This results from depositing the ferromagnet on top of an antiferromagnet. The conventional explanation is that the so-called ‘uncompensated spins’ (i.e. those which do not have partner spins to pair off with) in the antiferromagnet are exchange-coupled to the ferromagnetic spins across the interface, thereby shifting the hysteresis loop of the ferromagnet enough to keep its magnetization direction pinned even subject to relatively modest magnetic fields (~ 0.01 – 0.05 Tesla) [1] (figure 1). This pinning is achieved because the uncompensated spins in the antiferromagnet are strongly exchange-coupled to the bulk antiferromagnetic spins which do not reorient in these applied fields and are thus ‘frozen’ or ‘pinned’. However, basic unanswered questions remain about the detailed microscopic mechanism for exchange bias, including why the shift of the hysteresis loop is 2–3 orders of magnitude smaller than what a calculation of the idealized interface would suggest, where the uncompensated spins reside in the antiferromagnet, etc. and there have been several theoretical suggestions over the years about the effects of interface roughness, domain walls, disorder, etc. [2,3]. Clearly, a detailed microscopic probe of the spatial distribution of the magnetization on both sides of the ferromagnetic/antiferromagnetic interface would be extremely illuminating.

There have already been imaging studies of such interfaces with X-ray magnetic circular dichroism (XMCD) and magnetic photoelectron emission microscopy (PEEM) [4] which have revealed domains of uncompensated magnetization in the antiferromagnet at the interface, but these have not revealed the depth dependence of the magnetization. This precisely is what X-ray and neutron reflectivity can do. While these techniques do not yield direct images as many microscopy experiments do (e.g. atomic force microscopy, magnetic force microscopy, scanning tunneling microscopy, etc.), they do yield in a non-destructive fashion *global* statistical information about the sample and are particularly useful for probing *buried* interfaces. Resonant magnetic X-ray scattering occurs when the X-ray photon

energy is tuned (in the case of transition metals) to the L-edges for X-ray absorption for the element in question [5] and thus yields *element-specific* information about the magnetization, while neutron reflectivity yields the full vector components of the total magnetization as distributed in space.

In this paper, we present some combined neutron and magnetic resonant X-ray specular reflectivity results on an exchange bias system prepared by depositing a single crystal antiferromagnetic FeF₂ film epitaxially on a single crystal MgF₂ substrate and then depositing a polycrystalline ferromagnetic Co film on top, capped finally with a thin protective Al layer. This system, when cooled below the Neel temperature of FeF₂ in a field of 1 Tesla along the easy axis direction of the FeF₂ film, exhibits a positive exchange bias (hysteresis loop of Co is shifted along the field-cooled direction). Our analysis of these results indicate that there are in fact two kinds of uncompensated spins giving rise to net magnetization in the antiferromagnet, namely those that are pinned and those that can rotate in modest applied fields.

2. X-ray and neutron reflectivity

Reflectivity experiments (with X-rays or neutrons) measure the in-plane averaged depth profile of the scattering density from a surface or interface. In order to isolate the magnetic scattering component, it is often optimal to work with spin-polarized neutrons and use neutron polarization analysis for the reflected beam. If $R_{++}(Q_z)$ and $R_{--}(Q_z)$ represent the reflectivities for ‘up-spin’ and ‘down-spin’ neutrons specularly reflected as ‘up-spin’ and ‘down-spin’ neutrons respectively with wave vector transfer Q_z normal to the surface, and $R_{+-}(Q_z)$ represents reflectivity with spin-flip of the neutron, then we have

$$\begin{aligned} R_{++}(Q_z) - R_{--}(Q_z) &\sim M_{xy,\parallel}(Q_z)n(Q_z), \\ R_{+-}(Q_z) = R_{-+}(Q_z) &\sim |M_{xy,\perp}(Q_z)|^2, \end{aligned}$$

where $M_{xy,\parallel}(Q_z)$, $M_{xy,\perp}(Q_z)$ represent the Fourier components of the z -dependence of the components of the in-plane magnetization profile parallel and perpendicular to the neutron spin respectively and $n(Q_z)$ represents the Fourier component of the nuclear scattering length density. For these experiments both the sample magnetization and the neutron spin direction are in the plane of the film.

For resonant magnetic X-ray scattering, it is particularly important to eliminate the pure charge scattering, which is usually larger. The scattering factor for a single magnetic atom at resonance is given by [5]

$$\begin{aligned} f = \{ &(\mathbf{e}_s^* \cdot \mathbf{e}_i^*)(3\lambda/8\pi)[F_{11} + F_{1-1}] - r_s Z\} \\ &+ (3\lambda/8\pi)(\mathbf{e}_s^* \times \mathbf{e}_i^*) \cdot \mathbf{m}[F_{11} - F_{1-1}] \\ &+ (\mathbf{e}_s^* \cdot \mathbf{m})(\mathbf{e}_i^* \cdot \mathbf{m})[2F_{10} - F_{11} - F_{1-1}], \end{aligned}$$

where \mathbf{e}_s^* , \mathbf{e}_i^* are the polarization unit vectors of the scattered and incident photons respectively, \mathbf{m} is a unit vector along the magnetization of the atom, r_s is the Thompson scattering length of the electron, Z is the atomic number of the atom, and F_{10} , F_{11} and F_{1-1} are resonant matrix elements. The third term is small and

can often be neglected for scattering experiments. For circularly polarized photons at the resonant L-edge for that element, the specular reflectivity is different for the 2-senses of circular polarization relative to the magnetization direction, and in the Born approximation we may write [6,7]

$$R_+(Q_z) - R_-(Q_z) \sim M_{\parallel}(Q_z)n(Q_z),$$

where $M_{\parallel}(Q_z)$ is the Fourier component of the magnetization depth profile for that element projected along the incident beam direction and $n(Q_z)$ is the Fourier component of the charge depth profile as a function of depth z .

The above Born approximation-based expressions break down for small values of Q_z but more accurate expressions are available for an analysis of depth profiles from reflectivity measurements based on the so-called distorted wave Born approximation (DWBA) [7,8] or the so-called iterative matrix methods, and these have been used in the present analysis.

3. Experimental results

Exchange bias samples were prepared by sequential electron beam evaporation of FeF₂, Co and Al at a deposition rate of 0.05 nm/s onto (1 1 0) oriented single crystal MgF₂ polished substrates measuring 10 mm by 10 mm. The deposition temperatures were 300°C for the FeF₂ layer and 150°C for the Co and Al layers. The chemical structure of the sample was determined from an analysis of the sample's reflectivity acquired with non-resonant X-rays and was not subject to refinement in subsequent analyses of the resonant soft X-ray or neutron data. The thickness of the Co (FeF₂) layer was 4.1±0.1 nm (36.6±0.1 nm), and the structural roughness of the Co/FeF₂ (FeF₂/MgF₂) interface was 0.5±0.1 nm (0.4±0.1 nm). A comparison of the off-specular X-ray reflectivity and the specular X-ray reflectivity indicates that the roughnesses of the two interfaces were uncorrelated.

In-plane glancing angle X-ray diffraction and transmission electron microscopy confirmed that the AF layer was an untwinned single crystal film with [1 $\bar{1}$ 0]FeF₂ || [1 $\bar{1}$ 0]MgF₂, and surface normal along [1 1 0]FeF₂. The ~1.8° width of in-plane Bragg reflections from the FeF₂ single crystal was about four times broader than the reflections from the MgF₂ substrate. The dislocation density at the FeF₂/MgF₂ interface corresponds to an average spacing between dislocations of ~55 nm; however, were all the misfit strain in the FeF₂ film relieved, we would expect the spacing to be 21 nm. Therefore, only a fraction of the total misfit strain relieved is relieved in the FeF₂ film. Defects and strain (through piezomagnetism) can produce uncompensated magnetization in an antiferromagnet such as FeF₂.

The resonant soft X-ray scattering experiment was performed using a circularly polarized incident X-ray beam. The sample was cooled to 20 K in a field of $H_{FC} = 796$ kA/m (cooling field) applied along [0 0 1]FeF₂ (to establish bias). The sample and detector were rotated about [$\bar{1}$ 1 0]FeF₂. The intensity of the specularly reflected radiation was recorded as a function of incident beam polarization, applied field \vec{H} , and wave-vector transfer Q_z . The incident X-ray wavelength was tuned to either the Co-L₃ or Fe-L₃ edge such that the signs of the charge and magnetic scattering factors were the same. In the first measurement, we held the

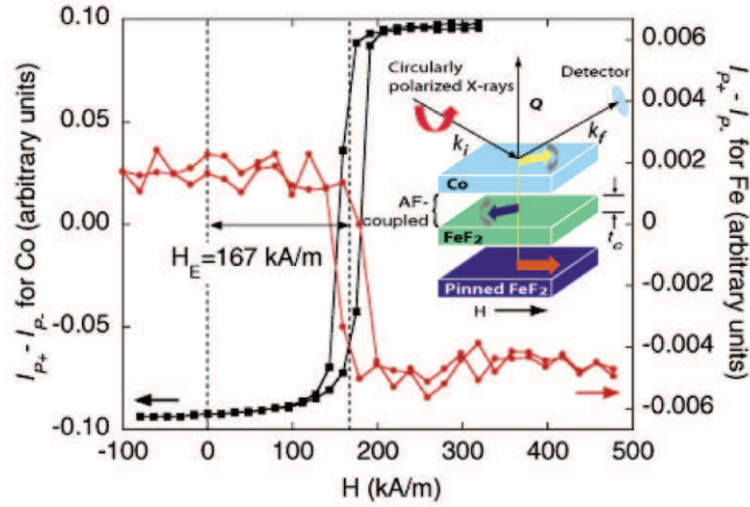


Figure 2. Hysteresis loops at $Q = 0.49$ and 0.38 nm^{-1} for Co (■) and Fe (●) respectively. Inset: Representations of the X-ray experiment and sample.

angles of incidence and reflection fixed at 3° (relative to the sample surface), and recorded the reflected intensity for left- and right-circularly polarized light, I_+ and I_- (polarization = $\pm 90\%$) as a function of H . Magnetization loops obtained from $I_+ - I_-$ (see figure 2) corresponding to Co (■, $Q = 0.49 \text{ nm}^{-1}$) or Fe (●, $Q = 0.38 \text{ nm}^{-1}$) spins exhibit hysteresis (see figure 2) indicating that some Co and Fe spins are unpinned. Both loops are shifted along the positive field axis (also parallel to H_{FC}) by the bias field, $H_E = 167 \pm 4 \text{ kA/m}$. Since the coercivity and bias obtained from either loop are the same, the Co and Fe spins are likely to be coupled. Along the magnetization axis, the curves are inverted – indicating that the Co and Fe spins are anti-parallel (for this Q).

We performed a second soft X-ray experiment that involved measuring the reflected beam intensity as a function of Q , for one incident X-ray beam polarization for $H = \pm 796 \text{ kA/m}$. This protocol is sensitive to changes in the specular reflectivity due to the reversal of unpinned spins. From the variation of I_{H+} and I_{H-} (the subscript refers to H being parallel (+) or anti-parallel (–) to H_{FC}) – the depth profiles of the Co and Fe spins can be obtained for each field direction. A theory for reflectometry with resonant X-ray beams based on a generalization of the distorted wave Born approximation was used to analyze the data. We chose to treat the Co magnetization as reversible in response to the applied field (i.e. ‘unpinned’), but retained the possibility for having both unpinned Fe spins which can respond to applied fields and Fe spins pinned along the direction of the cooling field. Using this model, the reflectivities for the two directions of H were calculated from the spin density profile shown to obtain the solid curves (inset) which are those yielding a best least squares fit (see figure 3). The spin profile represents the projection of the net magnetization of Co or Fe along the incident beam axis averaged over the x - y plane of the film. We see a change of the Fe spin magnetization from negative to positive values over a distance of $\sim 2 \text{ nm}$ below the Co/FeF₂ interface. We also

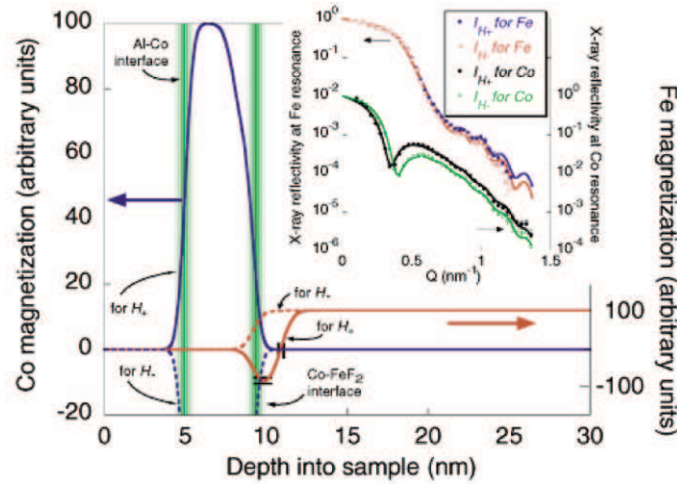


Figure 3. Spin density depth profiles for Co (blue) and Fe (red) spins obtained from the specular X-ray reflectivities (inset) at $H_{\pm} = \pm 796$ kA/m.

note a decrease in the magnetization density of Co as the Co/FeF₂ interface is approached. The changes in the projections of the Co and Fe spins along \vec{H} with depth occur over a distance much larger than that corresponding to interdiffusion or chemical roughness across the Co/FeF₂ interface, and thus can be explained by the presence of magnetic domains at the interface, or the rotation of magnetization away from the field axis.

We undertook a polarized neutron reflectometry study of the sample including polarization analysis in order to determine whether the spatial variation of the net magnetization vector in the Co and FeF₂ layers could be attributed to a domain wall parallel to the Co/FeF₂, and to obtain the depth profile of the pinned magnetization. After cooling the sample in a 438 kA/m field along $[0\ 0\ 1]\text{FeF}_2$ to 10 K (to establish bias), we rotated the sample about its surface normal in this field, so that \vec{H} was parallel to $[\bar{1}\ 1\ 0]\text{FeF}_2$ (inset). The intent of applying \vec{H} during the neutron measurement in a direction different from the cooling field (with a strength exceeding the anisotropy field of the sample) was to perturb the magnetization so that we could determine where the magnetization was pinned (in the direction of the cooling field) or unpinned. The polarized neutron reflectivity of the sample was analyzed after removing instrumental background and correction for polarization efficiencies. From measurements of $R_{++} - R_{--}$ and R_{+-} , as discussed in §2, the depth profile of the net magnetization vector projected onto the sample plane can be obtained quantitatively. The observation of non-zero SF reflectivity (proportional to the components of the net magnetization perpendicular to the original field-cooling direction, i.e. the direction of the incident neutron spins), implied that the field of 438 kA/m applied during the neutron measurement perpendicular to the cooling field axis $[0\ 0\ 1]$ was not sufficient to rotate the entire sample magnetization parallel to itself. We regard the portion of the magnetization that does not respond to field as pinned in the $[0\ 0\ 1]$ direction, since the field during the measurement

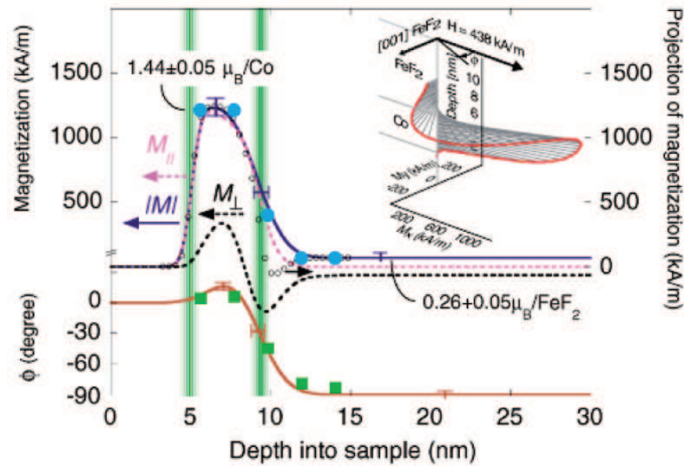


Figure 4. Depth dependence of the vector magnetization (inset, 3D view), magnitude (blue curve, $|M|$), and angular deviation ϕ (red curve) from the applied field in the sample plane deduced from neutron scattering. Error bars represent deviations of depth profiles with indistinguishable χ^2 . The magnetization used in the OOMMF simulation is indicated by \bullet and the values of ϕ are indicated by \blacksquare obtained from the simulation. The sum of the Fe and Co spin density profiles of $H||[001]\text{FeF}_2$ (obtained from figure 2 in arbitrary units using X-ray scattering) is shown in absolute units (\circ).

was applied along the $[\bar{1} 1 0]$ direction – a direction that was perpendicular to the cooling field.

We note that SF reflectivity was not observed when the field during the neutron measurement was applied parallel to the cooling field. Nor, was SF reflectivity observed when the measurement field was applied perpendicular to the cooling field and the temperature of the sample was 108 K – significantly above the ordering temperature $T_N = 78$ K of FeF_2 .

Quantitative information about the locations of unpinned and pinned uncompensated magnetization in the sample was obtained from an analysis of the Q dependence of the neutron reflectivity using the Parratt formalism. The magnetic structure of the model was divided into three regions representing magnetization in the Co layer (with magnitude M_{Co} and direction ϕ_{Co} , in the sample plane relative to the applied field), the interface (M_{int} , ϕ_{int}), and the FeF_2 bulk (M_{FeF_2} , ϕ_{FeF_2}). The magnetization of one region was connected to the next using an error function with width Δ (each magnetic interface had an adjustable width). The magnetic thickness of the interface was adjusted at the expense of the FeF_2 magnetic layer thickness. The model contains eight adjustable parameters, and these parameters were optimized to obtain the depth profiles shown from which R_{++} , R_{--} , and R_{+-} (solid curves), are obtained (see figure 4).

The magnetization in the Co film is mostly parallel to \vec{H} except near the Co/ FeF_2 interface where the magnetization rotates in the positive sense away from the applied field by $\phi_{\text{Co}} = +16^\circ$ (red curve), against the cooling field. The uncompensated

magnetization in the FeF₂ which rotates in the opposite sense is $\phi_{\text{int}} = -30^\circ$ near the Co/FeF₂ interface, and then perpendicular to the applied field in the FeF₂ bulk ($\phi_{\text{FeF}_2} = -89 \pm 5^\circ$). The tendency for the Co magnetization and the net uncompensated magnetization in the FeF₂ to rotate in opposition is evident in the change of sign of the component of the magnetization perpendicular to the applied field. The twist of the magnetization across the Co/FeF₂ interface is reminiscent of a domain wall parallel to the interface between soft and hard magnetic materials, as found for example in exchange spring magnets or in the computational model proposed by Kiwi *et al* [9] to explain exchange bias in Fe/FeF₂ bilayers. The rotation of the uncompensated magnetization close to the Co/FeF₂ interface provides a natural explanation for the experimental observation that an antiferromagnet must exceed a critical thickness, before bias is produced.

In a previous study of the influence of crystalline quality of FeF₂ films on exchange bias, exchange bias was found to be small for single crystal FeF₂ films grown on FeF₂ bulk single crystals – a recipe that minimizes misfit strain in the thin film lattice – in contrast to the substrate (MgF₂) used to make the sample reported presently. The accommodation of misfit strain through the formation of defects may be an important factor affecting the antiferromagnetic domain state and exchange bias. We note that previously large exchange bias in Co/Co_xO_{1-x} bilayers was attributed to uncompensated magnetization in the bulk of the non-stoichiometric CoO antiferromagnet.

We used the micromagnetic simulation package OOMMF to determine whether the magnetization profile deduced from neutron scattering was consistent with a low-energy magnetic configuration for the conditions of our experiment. We treated the interface and uncompensated spins in the FeF₂ layers as if they were slightly ferromagnetic, and assigned saturation magnetizations of 1212, 400 and 67 kA/m to the Co, interface and FeF₂ layers, respectively, to mimic the magnetization profile (● of figure 4). Values for the exchange stiffness of 30×10^{-12} and 1.23×10^{-12} J/m were used for Co and FeF₂, respectively, and the average of these values was assigned to the interface layer. Values for the uniaxial anisotropy of 4.5×10^5 and 1.76×10^6 J/m³ were used for Co and FeF₂, respectively. We included two adjustable parameters in the simulation – the interface exchange constant J_{int} across the Co-interface layers and the anisotropy of the interface K_{int} . Values of $J_{\text{int}} = -1.5 \times 10^{-3}$ to -2.0×10^{-3} J/m² and $K_{\text{int}} = 1 \times 10^5$ J/m³ yield the direction of the vector magnetization (■ of figure 4), and they are in good agreement with the neutron scattering result. The micromagnetic simulation was repeated using the same magnetic model, but with the field applied along [001]FeF₂ and varied between ± 477 kA/m. With the initial configuration of all three layers aligned in the positive direction, which is equivalent to cooling the sample in a large magnetic field, this simulation yielded a positively shifted hysteresis loop. This confirms that due to large anisotropy, the moments in the bulk FeF₂ remain pinned in the initial direction.

4. Conclusions

We have performed experiments that actively perturbed the magnetic structure of a Co/FeF₂ system – one exhibiting large exchange bias – in order to measure

the depth profiles of the pinned and unpinned magnetization. For a system with 167 kA/m exchange bias, we found that the antiferromagnetic FeF₂ layer possesses uncompensated magnetization. The uncompensated FeF₂ magnetization is antiparallel to the Co spins across the Co/FeF₂ interface, and the net uncompensated magnetization within 2 to 3.5 nm of this interface rotates in conjunction with the Co spins. Thus there is a strong antiferromagnetic coupling across the interface between Co spins in the ferromagnetic film and the Fe spins in a thin interface layer which are not strongly coupled to the bulk antiferromagnetic spins in the FeF₂. This coupling may be due to superexchange interactions via the F atoms at the interface. However, at distances greater than ~ 3.5 nm from the interface, the uncompensated FeF₂ magnetization is parallel to the original cooling field direction and pinned to the antiferromagnetic spins providing a means to establish bias. The fact that this bias is positive implies that these spins are coupled to the interface layer Fe spins ferromagnetically. Micromagnetic simulation confirms that the magnetization depth profile deduced from neutron reflectometry is a low-energy configuration, and the model structure yields a positively shifted hysteresis loop.

Acknowledgements

The facilities of the Manuel Lujan Jr. Neutron Scattering Center and the Advanced Light Source are gratefully appreciated. Discussions with M J Donahue, D Lederman, K Liu and R D McMichael are gratefully acknowledged. This work was supported in part by the Office of Basic Energy Science, US Department of Energy Grant DE-FG02-03ER46084 (SR and SKS), BES-DMS, the University of California Campus Laboratory Collaborative Program, and Laboratory Directed Research and Development Program funds. Also, financial support from the Alexander-von-Humboldt Foundation (OP), Cal(IT)² (Z-PL), Spanish MECD (RM and XB), Fulbright Commission (RM), Catalan Dursi (XB), and the Swiss National Science Foundation (MD) are acknowledged.

References

- [1] W H Meiklejohn and C P Bean, *Phys. Rev.* **105**, 904 (1957)
- [2] J Nogués and I K Schuller, *J. Magn. Magn. Mater.* **192**, 203 (1999)
- [3] A E Berkowitz and K Takano, *J. Magn. Magn. Mater.* **200**, 552 (1999)
- [4] H Ohldag *et al.*, *Phys. Rev. Lett.* **91**, 017203 (2003)
- [5] J P Hannon, G T Trammell, M Blume and D Gibbs, *Phys. Rev. Lett.* **61**, 1245 (1988)
- [6] R M Osgood, S K Sinha, J W Freeland, Y U Idzerda and S D Bader, *J. Magn. Magn. Mater.* **198–199**, 698 (1999)
- [7] D R Lee, S K Sinha, C S Nelson, J C Lang, C T Venkataraman, S Stepanov, G Srajer and R M Osgood, *Phys. Rev.* **B68**, 224410 (2003)
- [8] D R Lee, S K Sinha, D Haskel, Y Choi, J C Lang, S Stepanov and G Srajer, *Phys. Rev.* **B68**, 224409 (2003)
- [9] M Kiwi, *J. Magn. Magn. Mater.* **234**, 584 (2001)